

# Perpendicular transport and magnetization processes in magnetic multilayers with strongly and weakly coupled magnetic layers.

M. Zwierzycki<sup>†</sup> and S. Krompiewski

Institute of Molecular Physics, P.A.S Smoluchowskiego 17, 60-179 Poznań

April 26, 2024

## Abstract

Within the framework of a two-band tight-binding model, we have performed calculations of giant magnetoresistance, exchange coupling and thermoelectric power (TEP) for a system consisting of three magnetic layers separated by two non-magnetic spacers with the first two magnetic layers strongly antiferromagnetically exchange-coupled. We have shown how does the GMR relate with the corresponding regions of magnetic structure phase diagrams and computed some relevant hysteresis loops, too. The GMR may take negative values for specific layers thicknesses, and the TEP reveals quite pronounced oscillations around a negative bias.

PACS: 75.70.-i, 75.70.Pa, 75.60.Ej, 72.20.Pa

keywords: Giant magnetoresistance, Interlayer exchange coupling, Magnetization processes

---

<sup>†</sup>corresponding author, email: maz@ifmpan.poznan.pl

# 1 Introduction

Since the discovery of giant magnetoresistance (GMR) phenomenon in magnetic multilayers [1] there has been a great deal of interest in studying them by both theoretical and experimental methods. The reason for the interest is, already partially realized, possibility of practical applications as magnetic sensors, recording heads and magnetic memory elements.

The standard system exhibiting the GMR is a trilayer (*i.e.* two magnetic layers separated by a non-magnetic spacer) with thickness of the spacer chosen so as to produce antiferromagnetic coupling between magnetic layers. While such a system, due to its simplicity, is convenient for theoretical treatment, it presents some problems in practical applications. The main problem is a high switching field which is usually necessary to rotate the magnetizations (overcoming antiferromagnetic coupling) and produce GMR. One way to deal with this problem is to use somewhat more complex *spin-engineered* structures. Widely known structures of this type are spin-valve systems [2], in which one of the magnetic moments is fixed by the strong exchange coupling due to an additional antiferromagnetic layer (*e.g.* MnFe or CoO). There exists however also a different approach in which a system composed of three magnetic layers is used. Two of them are strongly antiferromagnetically coupled, forming the so called artificial antiferromagnetic subsystem (AAF) [3], and the third one — detection layer — is only weakly coupled (or just decoupled). Such a setup was proposed both for laboratory measurements [4, 5] and more practically as angular velocity meter [3]. A similar system (superlattice with strong and weak exchange couplings) was also studied theoretically (on *ab initio* level) [6], the thicknesses involved were however small due to numerical limitations.

The aim of the present paper is to perform thorough studies of transport and magnetic properties of the systems in question and to relate them with corresponding magnetic structure phase diagrams.

# 2 The model and the method of calculations

We consider a system consisting of three magnetic layers separated by two non-magnetic spacers, *i.e.* the structure of the  $F_1/S_1/F_2/S_2/F_3$  type, where  $F_i$  stands for ferro- and  $S_i$

for paramagnetic layer. In order to describe collinear configurations we employ tight-binding hamiltonian with two, hybridized bands and spin-dependent on-site potentials (see Ref. [7] for details). We restrict ourselves for simplicity to the case of simple cubic structure. The following values of model parameters have been chosen:  $E_F = 0$ ,  $t_s = -1$ ,  $t_d = -0.2$ ,  $V_{sd} = 1$ ,  $\epsilon_{i\sigma}^s = 0$ ,  $\epsilon_{i\uparrow}^d = -1$  for all the layers,  $\epsilon_{i\downarrow}^d = -0.2$  within magnetic layers and  $-1$  elsewhere, where  $E_F$  is the Fermi energy,  $t_\alpha$  (with  $\alpha$  being the band index —  $s, d$ ) are the hopping integrals,  $V_{sd}$  is the  $s - d$  intra-atomic hybridization and  $\epsilon_{i\sigma}^\alpha$  are the on-site potentials (where  $\sigma$  is  $\uparrow$  for majority- and  $\downarrow$  for minority-spin carriers). The above set of parameters enables us to mimic essential features of the electronic structure of Co/Cu multilayers (*i.e.* the spin-polarized density of states is qualitatively reproduced — in particular the majority  $d$ -bands in magnetic and (non-polarized)  $d$ -bands in paramagnetic layers are matched perfectly which closely resembles the situation in Co/Cu systems).

The conductance is computed from the Kubo formula with the help of recursion Green function technique [7, 8]. The only difference in comparison with [7] is that hybridization in lead wires (attached to the multilayer from both sides, for transport calculations) has been taken into account this time. The GMR has been defined as

$$\text{GMR} = \frac{\Gamma^{\uparrow\downarrow;\downarrow}}{\Gamma^{\uparrow\downarrow;\uparrow}} - 1, \quad (1)$$

where the arrows show the orientations of magnetic moments. Note that without the first magnetic layer this definition would be identical with the usual one. Additionally the thermopower (TEP) has also been calculated from the following formula (see eg. Ref. [9])

$$S = -\frac{\pi^2 k_B^2 T}{3|e|} \frac{d}{dE} \ln \Gamma(E). \quad (2)$$

We define, as in Ref. [10], the “giant magneto-TEP-effect” GMTEP analogously to Eq. (1) (with  $\Gamma$  replaced by  $S$ ).

For studying the magnetization processes we employ the phenomenological expression, not unlike the one introduced in Ref. [11], ( $\Theta_i$  is an angle between the  $i$ -th magnetic moment and

the external field,  $B$ )

$$\begin{aligned} E(\Theta_1, \Theta_2, \Theta_3) = & -J_{12} \cos(\Theta_1 - \Theta_2) - J_{23} \cos(\Theta_2 - \Theta_3) - J_{13} \cos(\Theta_1 - \Theta_3) \\ & - B \sum_{i=1}^3 t_i \cos(\Theta_i) / t + \sum_{i=1}^3 E_A(\Theta_i), \end{aligned} \quad (3)$$

where the first three terms describe bilinear exchange coupling between magnetic layers, the next three are Zeeman energy terms ( $t_i$  being  $i$ -th layer thickness and  $t$  the overall thickness of all the magnetic layers) and  $E_A(\Theta_i)$  is the crystalline anisotropy, that is  $t_i K \sin^2(2\Theta_i)/4t$  and  $-t_i D \cos^2 \Theta_i/t$  for cubic and uniaxial case respectively. We assume that external magnetic field is applied along the [10] in-plane crystallographic axis, which can be either easy or hard axis depending on the sign of the anisotropy constants. The magnetic moments are confined to the layers plane which corresponds to the strong shape anisotropy. Expression (3) was then numerically minimized, with respect to the  $\Theta_i$ -s, by taking, starting from initial configuration, little steps in the direction opposite to the energy gradient. All the extremal points found in this way were additionally checked against the stability condition (*i.e.* the positivity of all the minors of  $M_{ij} = \partial^2 E / (\partial \Theta_i \partial \Theta_j)$ ) in order to eliminate saddle points. Using Eq. (3) one can write (for  $B$  equal to 0)

$$\begin{aligned} J_{12} &= \frac{1}{4} [E(\pi 00) + E(0\pi 0) - E(000) - E(00\pi)], \\ J_{23} &= \frac{1}{4} [E(00\pi) + E(0\pi 0) - E(000) - E(\pi 00)], \\ J_{13} &= \frac{1}{4} [E(00\pi) + E(\pi 00) - E(000) - E(0\pi 0)]. \end{aligned} \quad (4)$$

Therefore, having known the energies of collinear configurations from the model calculations (based on the two-band tight-binding hamiltonian), we are able to determine the exchange coupling constants.

From now on we will be using reduced values of the magnetic field  $b = B/|J_{12}|$  and the anisotropy constants  $k = K/|J_{12}|$  and  $d = D/|J_{12}|$ . We will also assume, if not stated explicitly otherwise, the magnetic layers thicknesses to be 8, 3 and 3 ML (monolayers), respectively, in order to keep the length ratios as in Ref. [5]. The first spacer thickness will be set to 3 ML in

order to achieve the needed antiferromagnetic coupling between the first two magnetic layers.

### 3 Results

Figure 1 presents the exchange coupling constants ( $J$ -s) plotted against the thickness of the second spacer ( $ns_2$ ). As mentioned above, for the chosen thicknesses we got strong antiferromagnetic coupling ( $J_{12}$ ) between the first two magnetic layers, while  $J_{23}$  and  $J_{13}$  oscillate around zero. In all three cases the period of oscillations is about 3 ML, which is close to the theoretically predicted value (2.8 ML) coming from the stationary spanning vector [12, 13] placed at the  $(0, \pi)$  (and equivalent positions) in the two-dimensional Brillouin zone. The second period (8 ML) originating from the hole pocket placed at  $(\pi, \pi)$  does not seem to appear in the present context. Note however that it can become visible under some circumstances like in Ref. [7] where the tunnelling conductance has been considered. The GMR and  $J_{23}$  for the same system have been plotted in Fig. 2. It can be noted that GMR asymptotically tends to oscillate with the same period but in opposite phase to  $J_{23}$ . This is in agreement with our previous findings [13], but it is still not clear to what extent this correlation is universal. The values of GMR are strongly reduced in comparison with the trilayer case. This can be easily understood if we note that, due to the fixed antiferromagnetic alignment of the first two magnetic layers, there is no non-scattering channel in any of the configurations involved (see Eq. 1). Figure 3 where the on-site potentials for the  $d$ -bands ( $\epsilon_{i\sigma}^d$ ) have been schematically plotted, shows that there exist at least two scattering interfaces in each case. Basing on the number of interfaces one can qualitatively predict that the  $\uparrow\downarrow; \downarrow$  down- and  $\uparrow\downarrow; \uparrow$  up-spin electron channels have the higher conductances than the remaining two. This is indeed clearly visible in Fig. 4 where the computed conductances are shown. As already discussed there is no obvious highest conductance channel. Instead, we have two higher and two lower conducting channels close to each other within the pairs. As a consequence the sign of GMR is determined by all the channels, and can be changed by manipulating some parameters (eg. thicknesses of the layers). This is the case in Fig. 5 where we have plotted the GMR and  $J_{23}$  for a system with thickness of the second magnetic layer set to 5 ML (instead of 3 ML

as in Fig. 2). The GMR oscillations have a small but clearly negative bias. The asymptotic opposite-phase correlation with respect to  $J_{23}$  is again clear in this case.

The GMTEP, calculated for the same set of parameters as in Fig. 2, has been plotted in Fig. 6. In agreement with the findings of Ref. [10], the oscillations are quite pronounced and have the same period as GMR but exhibit negative bias. Asymptotically they seem to have roughly the same phase as GMR.

For studying the magnetization processes we have chosen the parameters as in Fig. 1 with the second spacer thickness ( $ns_2$ ) set to 7 ML (the second ferromagnetic maximum of  $J_{23}$ ). As already stated, two cases have been taken into account, *i.e.* the cubic and uniaxial anisotropies.

In the first case the anisotropy term ( $t_i k \sin^2(2\Theta_i)/4t$ ) gives rise to four potential wells placed at the following in-plane crystallographic axes : [10], [01], [ $\bar{1}0$ ] and [0 $\bar{1}$ ] for  $k > 0$  and [11], [ $\bar{1}\bar{1}$ ], [ $\bar{1}\bar{1}$ ] and [1 $\bar{1}$ ] for  $k < 0$ . Figure 7a exemplifies some phase diagrams for various initial configurations. We have chosen the simplest ones *i.e.* the collinear configurations with relative alignment of magnetic moments favoured by interlayer exchange coupling. It is however, in principal, possible to stabilize also non-collinear ones, provided that the anisotropy is strong enough. The phase diagrams have been obtained by taking subsequent scans along  $b$  for different  $k$  values. Dotted horizontal lines are thus only guides to the eye. The diagrams exhibit rich structure with a number of configurations (phases) occurring during the magnetization process (including the non-collinear configurations). The transition between them can be either of first or second type, that is they manifest themselves as discontinuities in magnetization or its first derivative. Some exemplary hysteresis loops are presented in Fig. 7b. As expected stronger anisotropy produces a richer structure. For positive, and sufficiently big, values of  $k$  some flat regions, typical for exchange-biased systems, occur. Note however that there is no  $\uparrow\downarrow;\downarrow$  to  $\uparrow\downarrow;\uparrow$  transition in the first diagram of Fig. 7a (but see below).

For the case of uniaxial anisotropy ( $-t_i d \cos^2(\Theta_i)/t$ ) there exist only two potential wells, that is [10] and [ $\bar{1}0$ ] for  $d > 0$  and [0 $\bar{1}$ ], [01] for  $d < 0$ . The phase diagrams (Fig. 8a) are somewhat less complicated now, due to the simpler energy landscape. The saturation curve for the upper part of the first diagram (with the  $\uparrow\downarrow;\downarrow$  initial configuration) has been obtained on analytical basis (*i.e.* from the stability condition) because of the weak stability of the  $\uparrow\downarrow;\uparrow$

configuration (by which we mean that the existing energy minimum is very shallow) which makes it difficult to perform reliable numerical minimalization. The same precautions have been applied to the first hysteresis loop in Fig. 8b. Note that this time the flat regions are present already for small values of  $d$ . For  $d > 0.51$  there exists, in the first diagram, the above mentioned  $\uparrow\downarrow; \downarrow$  to  $\uparrow\downarrow; \uparrow$  transition. Only positive values of  $d$  were presented since the opposite case is trivial — there is practically no hysteresis.

## 4 Conclusions

Within the microscopic two-band tight-binding model we have performed the calculations of interlayer exchange coupling, current-perpendicular-to-plane conductance and thermopower for a system consisting of three magnetic layers, separated by paramagnetic ones. With the thicknesses chosen so as to produce strong antiferromagnetic coupling between the first two magnetic layers, we found both the interlayer exchange coupling, GMR and GMTEP to oscillate, as a function of the second spacer thickness, with the period originating from one of the extremal spanning vectors of the Fermi surface. Additionally, using the phenomenological approach, we have computed magnetic phase diagrams and commented on their relevance to the magnetoresistance. We found that the phase diagrams exhibit rich structure and there are flat regions in hysteresis loops, typical for exchange-biased spin-valves. It has been also found that in the case of the systems under consideration, in contrast to conventional trilayers, it is possible to obtain a negative (inverse) perpendicular GMR by merely changing thicknesses of particular layers.

## 5 Acknowledgments

The KBN grants 2PO3B-118-14 and 2PO3B-117-14 are gratefully acknowledged. We also thank Poznań Computing and Networking Center for the computing time.

## References

- [1] G. Binasch, P. Grünberg, F. Sauerbach, and W. Zinn, Phys. Rev. B 39 (1989) 4828.
- [2] B. Dieny, V.S. Sperious, S. Metin, S.S.P. Parkin, B.A. Gurney, P. Baumgart, and D.R. Wilhoit, J. Appl. Phys. 69 (1991) 4774.
- [3] H.A.M. van den Berg, W. Clemens, G. Gieres, G. Rupp, M. Vieth, J. Wecker, S. Zoll, J. Magn. Magn. Mater. 165 (1997) 524.
- [4] S.S.P. Parkin and D. Mauri, Phys. Rev. B 44 (1991) 7131.
- [5] P.J.H. Bloemen, R. van Dalen, W.J.M. de Jonge, M.T. Johnson, and J. aan de Stegge, J. Appl. Phys. 73 (1993) 5972.
- [6] S. Krompiewski, F. Süss, U. Krey, J. Magn. Magn. Mater. 164 (1996) L263.
- [7] S. Krompiewski and U. Krey, Europhys. Lett. 44 (1998) 661.
- [8] Y. Asano, A. Oguri, J. Inoue, and S. Maekawa, J. Magn. Magn. Mater. 136 (1994) L18.
- [9] N.F. Mott and E.A. Davis, *Electronic Properties in Non-Crystalline Materials* (Clarendon Press, Oxford, 1979), Chap. 2.13.
- [10] S. Krompiewski and U. Krey, Phys. Rev. B 54 (1996) 11961.
- [11] W. Schmidt, J. Magn. Magn. Mater. 84 (1990) 119.
- [12] P. Bruno, Phys. Rev. B 52 (1995) 411.
- [13] S. Krompiewski, M. Zwierzycki and U. Krey, J. Phys.: Condens. Matter. 9 (1997) 7135.

# List of Figures

1	Exchange coupling constants, calculated for the $F_1/S_1/F_2/S_2/F_3$ structure, plotted against the second spacer thickness ( $ns_2$ ). Magnetic layer thicknesses have been set to 8, 3 and 3 ML, respectively and the first spacer thickness is equal to 3 ML. The hamiltonian parameters are as follows: $E_F = 0$ (Fermi energy), $t_s = -1$ , $t_d = -0.2$ (hopping integrals), $V_{sd} = 1$ (hybridization), $\epsilon_{i\sigma}^s = 0$ and $\epsilon_{i\uparrow}^d = -1$ (for all the layers), $\epsilon_{i\downarrow}^d = -0.2$ for $i$ within the magnetic layer and $-1$ elsewhere. Note the strong antiferromagnetic coupling ( $J_{12}$ ) between the first two magnetic layers. . . . .	11
2	CPP-GMR and the interlayer exchange coupling ( $J_{23}$ ) plotted as a function of the second spacer thickness. The period of oscillation is about 3 ML in agreement with the predicted value of 2.8 ML, resulting from the corresponding Fermi surface calliper. Asymptotically the oscillations of both quantities are predominantly opposite in phase. . . . .	12
3	Schematic plot of the on-site potentials for $d$ -bands ( $\epsilon_{i\sigma}^d$ ) across the $F_1/S_1/F_2/S_2/F_3$ multilayer for different configurations and spin directions. The $\uparrow\downarrow; \downarrow$ down- and $\uparrow\downarrow; \uparrow$ up-spin channels with only two scattering interfaces are clear candidates for high conductance channels. Note that there is however no non-scattering channel for configurations taken into account. . . . .	13
4	Conductances (in $e^2/h$ units) for parameters as in Fig. 2. There exist, as discussed in the text, two high and two low conductance channels. . . . .	13
5	CPP-GMR and the interlayer exchange coupling ( $J_{23}$ ) calculated for the same set of parameters as in Fig. 2, except for the thickness of the second magnetic layer ( $nf_2$ ) which has been set to 5 ML. The GMR oscillate around a small <i>negative</i> value. . . . .	14
6	GMTEP (giant magneto-TEP effect) for the same set of parameters as in Fig. 2. GMR has been also plotted for reference. The GMTEP oscillates asymptotically in roughly the same phase but around a negative bias. . . . .	15

7	a) Phase diagrams for magnetization processes obtained for different initial configurations in the case of cubic anisotropy. The second spacer thickness ( $ns_2$ ) has been set to 7 ML. The arrangements of magnetic moments are schematically drawn with the first (8 ML) magnetic layer symbolized by the long solid arrow and the third one (detection layer) by the dotted arrow. b) Exemplary hysteresis loops with the dashed line marking the backward sweep. The zero field configurations are schematically marked for both the sweep directions. For positive values of $k$ , the strong anisotropy produces flat regions typical for exchange-biased systems. . . . .	15
8	a) Phase diagrams in the uniaxial anisotropy case. b) Exemplary hysteresis loops. Only positive values of $d$ are shown since the opposite case exhibits no hysteresis at all. The flat regions are present already for weak anisotropy. . . .	16

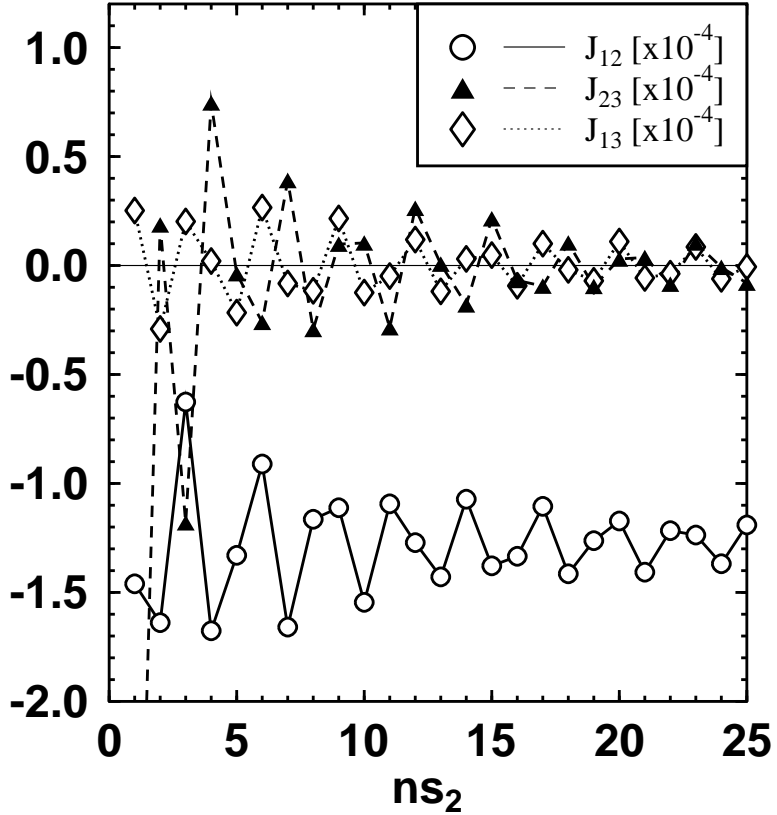


Figure 1: Exchange coupling constants, calculated for the  $F_1/S_1/F_2/S_2/F_3$  structure, plotted against the second spacer thickness ( $ns_2$ ). Magnetic layer thicknesses have been set to 8, 3 and 3 ML, respectively and the first spacer thickness is equal to 3 ML. The hamiltonian parameters are as follows:  $E_F = 0$  (Fermi energy),  $t_s = -1$ ,  $t_d = -0.2$  (hopping integrals),  $V_{sd} = 1$  (hybridization),  $\epsilon_{i\sigma}^s = 0$  and  $\epsilon_{i\uparrow}^d = -1$  (for all the layers),  $\epsilon_{i\downarrow}^d = -0.2$  for  $i$  within the magnetic layer and  $-1$  elsewhere. Note the strong antiferromagnetic coupling ( $J_{12}$ ) between the first two magnetic layers.

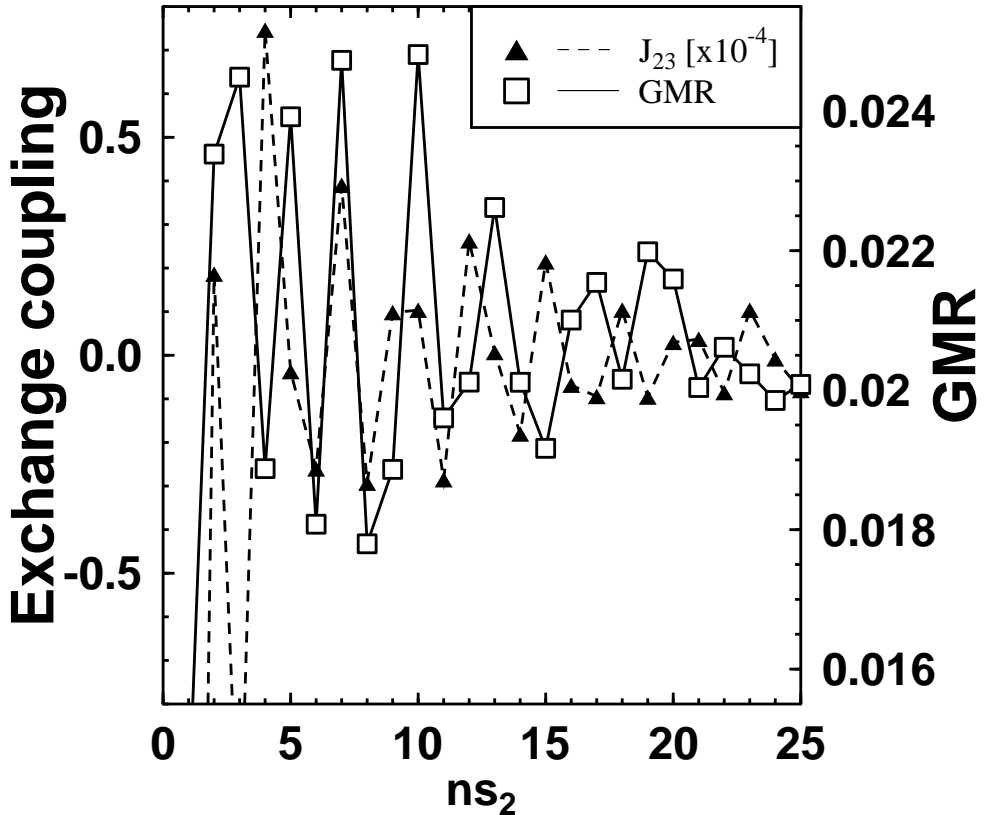


Figure 2: CPP-GMR and the interlayer exchange coupling ( $J_{23}$ ) plotted as a function of the second spacer thickness. The period of oscillation is about 3 ML in agreement with the predicted value of 2.8 ML, resulting from the corresponding Fermi surface calliper. Asymptotically the oscillations of both quantities are predominantly opposite in phase.

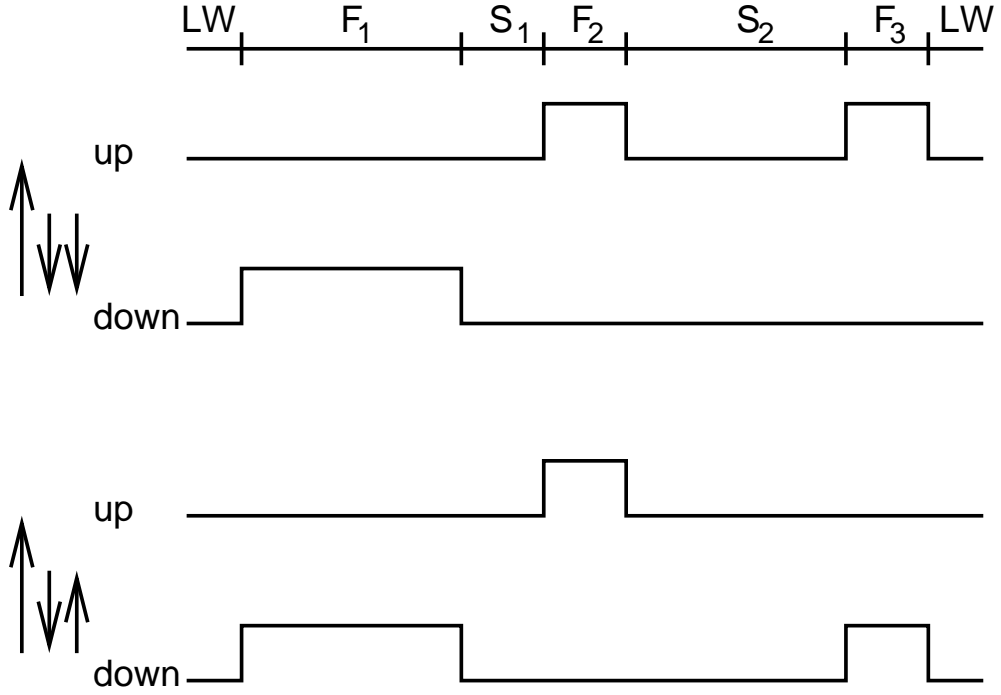


Figure 3: Schematic plot of the on-site potentials for  $d$ -bands ( $\epsilon_{i\sigma}^d$ ) across the  $F_1/S_1/F_2/S_2/F_3$  multilayer for different configurations and spin directions. The  $\uparrow\downarrow; \downarrow$  down- and  $\uparrow\downarrow; \uparrow$  up-spin channels with only two scattering interfaces are clear candidates for high conductance channels. Note that there is however no non-scattering channel for configurations taken into account.

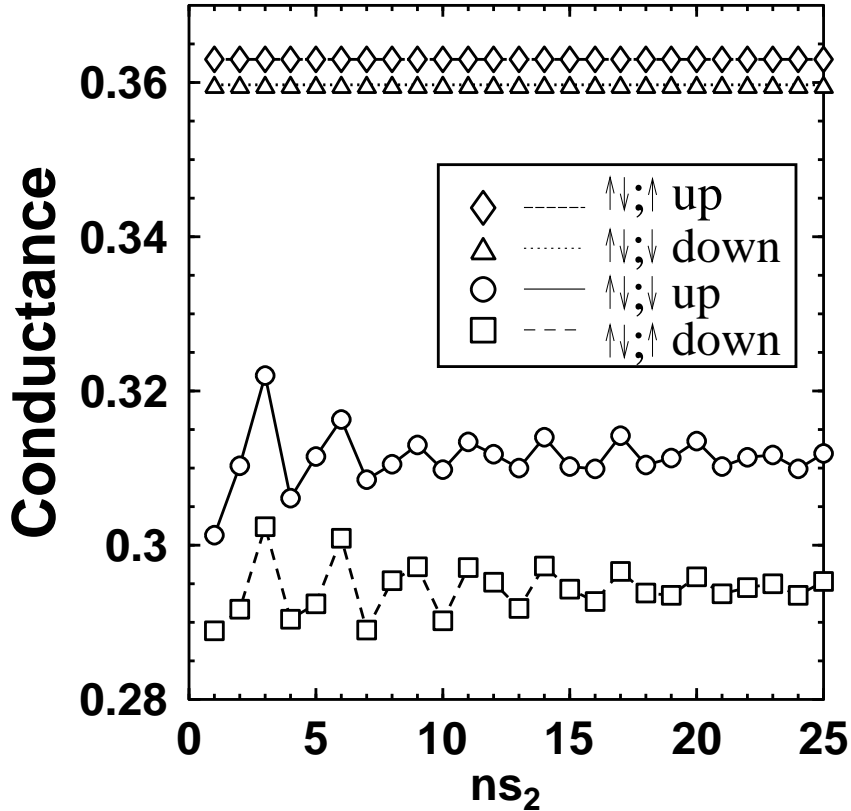


Figure 4: Conductances (in  $e^2/h$  units) for parameters as in Fig. 2. There exist, as discussed in the text, two high and two low conductance channels.

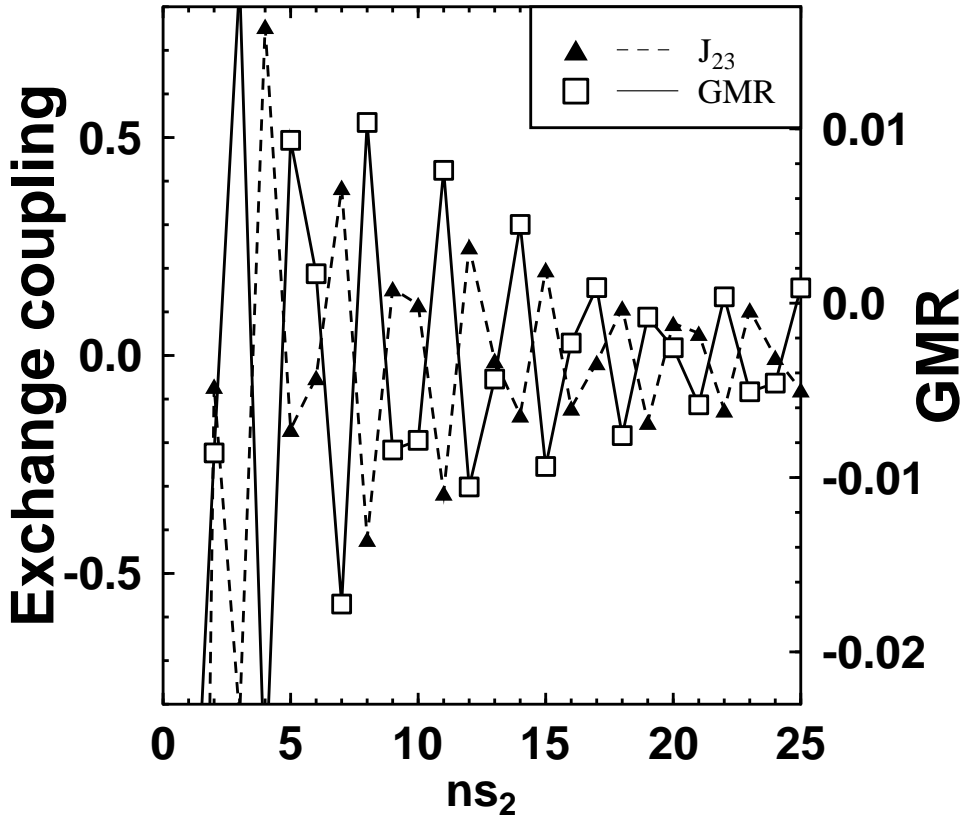


Figure 5: CPP-GMR and the interlayer exchange coupling ( $J_{23}$ ) calculated for the same set of parameters as in Fig. 2, except for the thickness of the second magnetic layer ( $nf_2$ ) which has been set to 5 ML. The GMR oscillate around a small *negative* value.

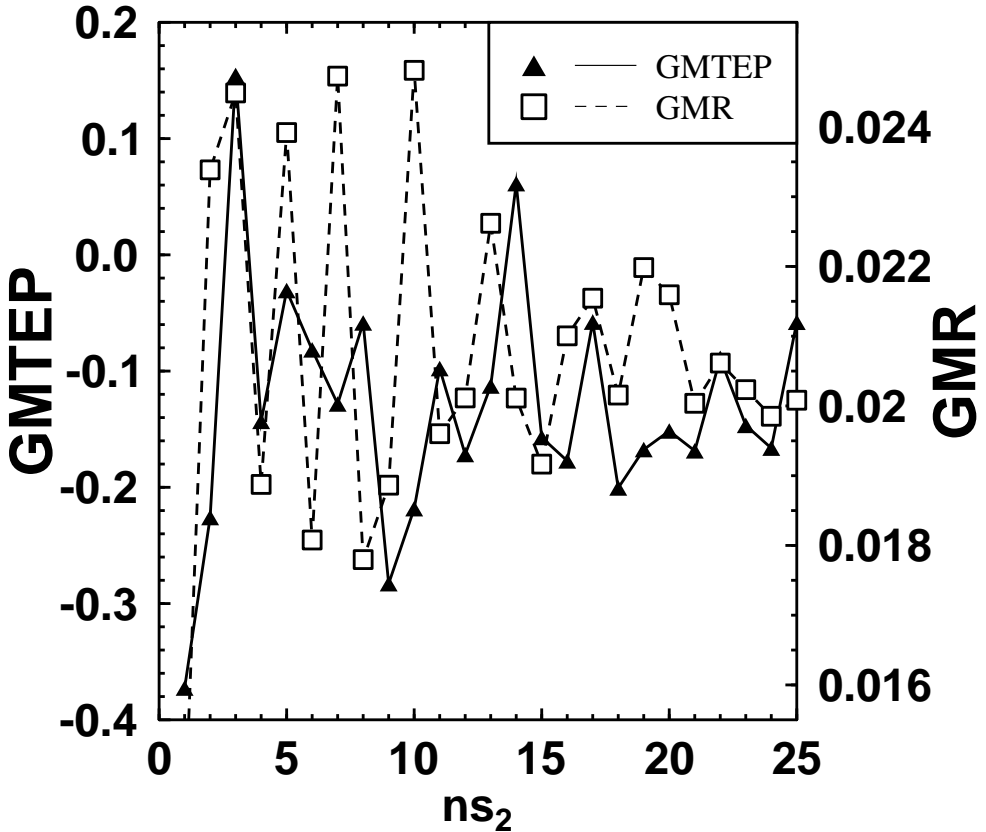


Figure 6: GMTEP (giant magneto-TEP effect) for the same set of parameters as in Fig. 2. GMR has been also plotted for reference. The GMTEP oscillates asymptotically in roughly the same phase but around a negative bias.

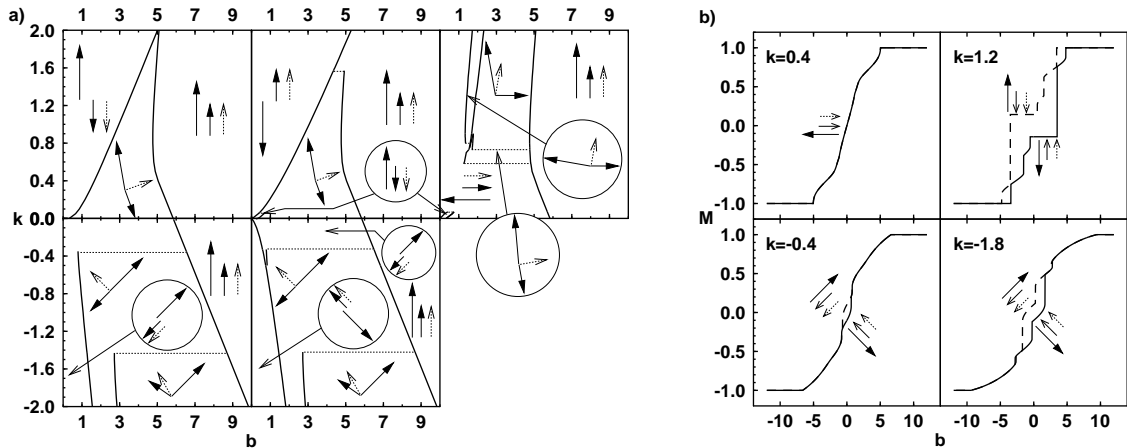


Figure 7: a) Phase diagrams for magnetization processes obtained for different initial configurations in the case of cubic anisotropy. The second spacer thickness ( $nS_2$ ) has been set to 7 ML. The arrangements of magnetic moments are schematically drawn with the first (8 ML) magnetic layer symbolized by the long solid arrow and the third one (detection layer) by the dotted arrow. b) Exemplary hysteresis loops with the dashed line marking the backward sweep. The zero field configurations are schematically marked for both the sweep directions. For positive values of  $k$ , the strong anisotropy produces flat regions typical for exchange-biased systems.

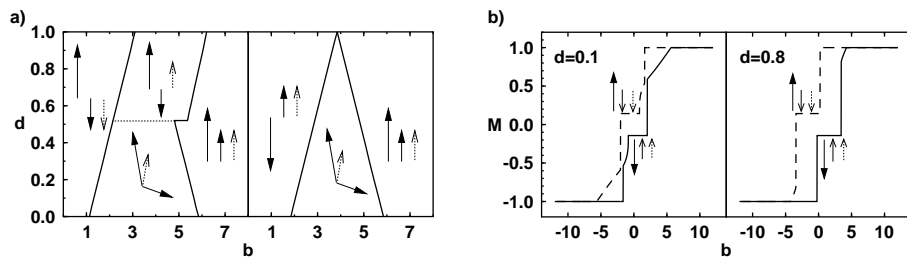


Figure 8: a) Phase diagrams in the uniaxial anisotropy case. b) Exemplary hysteresis loops. Only positive values of  $d$  are shown since the opposite case exhibits no hysteresis at all. The flat regions are present already for weak anisotropy.